J. Fluid Mech. (1976), *vol.* 76, *part* 3, *pp.* 561–592
Printed in Great Britain

The modelling of large eddies in a two-dimensional shear layer

By E. ACTON
Engineering Department, University of Cambridge

(Received 15 September 1975)

Large coherent eddies have been observed in turbulent shear layers and seem to play an important role in their growth, mixing and noise production. Winant & Browand (1974) have observed that the pairing of large eddies is central to the question of shear-layer development, and they model the pairing process with discrete line vortices. It is shown here that the growth of the layer and amalgamation of large eddies are not adequately treated by isolated-line-vortex models, which are proved to be essentially non-evolutionary. A more detailed model of the shear layer, itself consisting of vortex elements, is shown to provide the definition required to observe the evolution and coalescence of the large eddies. The observed development of this model shear layer is consistent with many features of experimentally observed flows.

1. Introduction

In recent years, visualization experiments on turbulent shear flows have revealed a large-scale structure which had not previously been apparent from statistical measurements. These large eddies now seem to play an important role in shear-layer growth, turbulent mixing and noise production; this paper describes some models through which certain aspects of their behaviour can be studied and quantified.

Crow & Champagne (1971) suggested that turbulence in a round jet contained significant orderly structure. They observed that jet instability gave rise to a train of loosely packed vortex rings which tended to retain their identity as they travelled downstream. More recently, Lau & Fisher (1975) have confirmed that the dominant structure in the first few diameters of a round jet consists of an axial array of such vortices.

In an experimental study of a two-dimensional turbulent mixing layer between streams of two different gases, Brown & Roshko (1974) have observed a large-scale coherent eddy structure that is similar to that observed in the nonlinear stages of the transition of a laminar shear layer. Much experimental and theoretical work has confirmed that the laminar shear layer can roll up into vortices (Michalke 1970). Freymuth (1966) was able to categorize the various stages of development of shear-layer transition at high Reynolds number. Transition excited by sound began at the nozzle edge, downstream of which disturbances grew exponentially. A nonlinear region followed which was clearly visible with

smoke visualization. The vortices were seen to roll around one another and coalesce. Neither the linear nor nonlinear regions were much affected by viscosity.

It is probable that the large eddies are the debris of the initially unstable flow, and have developed to such a stage that they determine the mean flow structure.

From the experiments of Brown & Roshko it is apparent that, in agreement with the similarity laws, the eddy spacing and scale increase linearly with downstream distance. As individual eddies are observed to move downstream at an approximately constant velocity, the linear increase cannot be a continuous process. There must be some way in which eddies can lose their identity as they convect downstream. One possibility is the vortex coalescence observed by Freymuth. This was seen through smoke pictures and also from the appearance of subharmonics of the primary instability frequency. Subsequent downstream repetitions of this merging, occurring randomly in time and space, produce a statistically smooth, linearly growing mixing layer.

Experiments on the mixing layer at moderate Reynolds number have been reported recently by Winant & Browand (1974). They mixed a high velocity water flow with a slower stream, behind a splitter plate. The interface was visualized with dye. The formation of vorticity concentrations from growing, but initially weak waves was similar to that observed by Freymuth. But in the subsequent development, vortices interacted by rolling around one another and coalesced to form single larger vortices with approximately twice the former spacing. It is this interaction which is seen to control the spreading rate of the turbulent mixing layer. Similar coalescence which persists into the fully developed turbulent region was observed in round jets by Laufer (1974) and in planar jets by Rockwell & Niccolls (1972), who also felt that this was the controlling mechanism for growth.

An identification of the large eddies as governing the flow development provides a useful, almost deterministic picture of important elements in turbulence. Large fast eddies are the main cause of noise (Lighthill 1952), and the idea that they might be relatively deterministic, and therefore controllable, is extremely important. Indeed, Laufer proposes a quasi-ordered compact source model based on eddy coalescence. A deceleration observed (Laufer 1974) to precede pairing in a round jet indicates that the outer ring expands and slows whilst the inner ring contracts and accelerates to catch it up. This is a relatively sudden large-scale event, which must cause efficient sound production. This process would occur in the early stages of jet development and it is there that the most intense jet-noise production is known to occur (Kinns 1975).

The large eddies also provide a clearer understanding of the process of entrainment. The pictures and measurements of density fluctuations made by Brown & Roshko suggest that turbulent mixing and entrainment is a process of entanglement on the scale of the large structures. The eddies engulf fluid in their formation but during their lifetime are subject to internal mixing only while the eddy is transporting fluid from both sides of the mixing layer.

Since large eddies have such an importance it is of considerable interest to attempt to model the amalgamation process, and to consider whether coalescence is an essential or likely interaction between two vortices.

Initial steps in modelling this were taken by computing the paths of two line-vortex pairs. It became clear from the numerical computations that the motion for vortices of the same sign was nearly always periodic. Love's (1894) classical analysis of this problem (with vortices of equal strength) is extended in §2 to include unequal strengths. There it is shown that there exists a condition for cyclic motion which relates the ratio of the breadths of the two vortex pairs at the time when they pass one another. The paths taken by the vortices are determinable from their initial positions. Typical paths for the cyclic motion are shown in figures 4 and 5. The motion of two vortices of opposite sign is not periodic and eventually the vortex pairs move away from each other. A third vortex pair can, however, act to make two other vortex pairs not initially set in periodic motion move into cyclic motion.

A model proposed by Winant & Browand consists of two equi-spaced infinite arrays of line vortices, members of which can never become locked in cyclic motion (figure 18). Thus, notwithstanding our observation of 'catalytic pairing' and Winant & Browand's suggestion to the contrary, the main conclusion to be drawn from this part of the paper is that the motion of simple configurations of isolated line vortices is essentially non-evolutionary and cannot adequately model the interactions which occur in the shear layer.

A model which can represent more details of the vortices involved in these interactions is clearly required. Such a model is described in §3, where discrete line vortices are used to represent a shear layer. The growth of this shear layer is computed and finite-area concentrations of vorticity evolve. These eddies are then seen to interact by rolling around one another and coalescing. The development of these vortices and their subsequent amalgamation are shown in figure 10. A systematic variation of the parameters used to define the initial shear layer shows that, although the formation of the first eddies is dependent on the initial conditions, the occurrence and abruptness of the amalgamation process depend only on the irregularity in lateral spacing of the structures. It is seen from this computation that the amalgamation of eddies by rotation and pairing can be inviscidly modelled to provide a growth mechanism of the shear layer. It is also possible to model in this way the growth mechanism proposed by Moore & Saffman (1975), where eddy destruction takes place when two strong vortices are able to tear apart a weak neighbour. But we observed in our computations that the amalgamation by rotation and pairing is more likely to occur, presumably because it depends on ever present irregularities in lateral spacing. The abruptness of this modelled process is clearly visible in our results; such a rapid change with a large length scale is inevitably a less compact motion than the bulk of turbulence and this makes it a much more effective noise source. It is also clear from the figures that this technologically important motion is both relatively deterministic and clearly identifiable with commonly visualized aspects of shear flow.

2. The kinematics of discrete vortex pairs

The simplest formulation of the vortex interaction problem is the relative motion of two line-vortex pairs. This is considered here to discover whether two such pairs have an essentially independent existence or whether they interact and evolve into a 'paired' situation where the four vortices are locked in cyclic motion.

The stream function ψ due to a line vortex of strength κ_0 at the position (x_0, y_0) is

$$\psi(x,y) = (-\kappa_0/4\pi)\log_e[(x-x_0)^2+(y-y_0)^2].$$

The stream function for the vortex configuration illustrated in figure 1 is obtained by superposition:

$$\psi(x,y) = \frac{\kappa_0}{4\pi}\log_e\left(\frac{(x-x_0)^2+(y+y_0)^2}{(x-x_0)^2+(y-y_0)^2}\right)+\frac{\kappa_1}{4\pi}\log_e\left(\frac{(x-x_1)^2+(y+y_1)^2}{(x-x_1)^2+(y-y_1)^2}\right),$$

where, of course, x_0 and y_0 are now time dependent.

For a system of vortex pairs the theory of the impulse (Lamb 1924, art. 157) leads to

$$\Sigma\kappa y = \text{constant}.$$

This can be written as

$$\bar{y} = (\kappa_1 y_1 + \kappa_0 y_0)/(\kappa_1+\kappa_0), \tag{1}$$

where $\bar{y} = c = \text{constant}$. The energy of the motion (Lamb, art. 157) is given by

$$T = -\tfrac{1}{2}\rho\Sigma\kappa\psi = \text{constant}.$$

From this, the generalization of Love's (1894) equation (5) readily follows:

$$y_1^{\kappa_1/\kappa_0}y_0^{\kappa_0/\kappa_1}\left(\frac{(x_1-x_0)^2+(y_1+y_0)^2}{(x_1-x_0)^2+(y_1-y_0)^2}\right) = k^2 = \text{constant}. \tag{2}$$

The components of the vortex convection velocity are obtained from the stream function:

$$\frac{dx_1}{dt} = -\frac{\kappa_0(y_1-y_0)}{2\pi[(x_1-x_0)^2+(y_1-y_0)^2]}+\frac{\kappa_0(y_1+y_0)}{2\pi[(x_1-x_0)^2+(y_1+y_0)^2]}+\frac{\kappa_1}{4\pi y_1}, \tag{3a}$$

$$\frac{dy_1}{dt} = \frac{\kappa_0(x_1-x_0)}{2\pi[(x_1-x_0)^2+(y_1-y_0)^2]}-\frac{\kappa_0(x_1-x_0)}{2\pi[(x_1-x_0)^2+(y_1+y_0)^2]}, \tag{3b}$$

$$\frac{dx_0}{dt} = \frac{\kappa_1(y_1-y_0)}{2\pi[(x_1-x_0)^2+(y_1-y_0)^2]}+\frac{\kappa_1(y_1+y_0)}{2\pi[(x_1-x_0)^2+(y_1+y_0)^2]}+\frac{\kappa_0}{4\pi y_0}, \tag{3c}$$

$$\frac{dy_0}{dt} = \frac{-\kappa_1(x_1-x_0)}{2\pi[(x_1-x_0)^2+(y_1-y_0)^2]}+\frac{\kappa_1(x_1-x_0)}{2\pi[(x_1-x_0)^2+(y_1+y_0)^2]}. \tag{3d}$$

Consider the vortices to be rotating about the 'centre' $(\bar{x}, \bar{y})$ of the system of vortices (Lamb, art. 154) as shown in figure 2. Then

$$\bar{y} = c = \text{constant} \quad \text{from (1)},$$
$$\bar{x} = (\kappa_0 x_0 + \kappa_1 x_1)/(\kappa_0+\kappa_1) \neq \text{constant}.$$

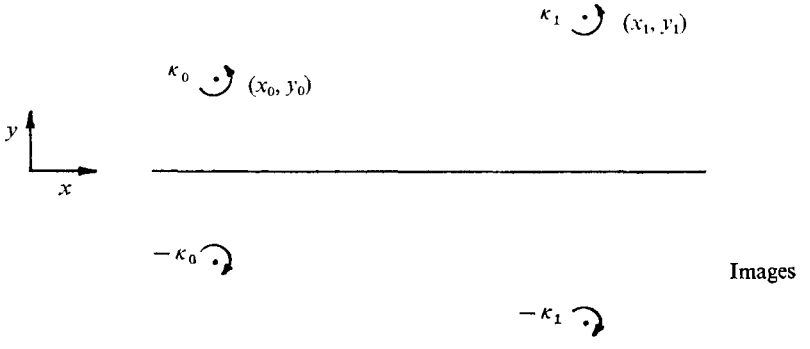

FIGURE 1. Initial positions of vortex-line pairs.

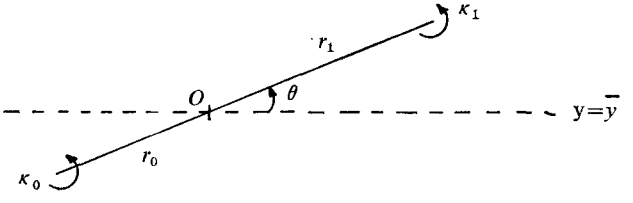

FIGURE 2. Relative positions of vortex half-pairs.

Using the notation of the figure

$$y_1 = r_1 \sin\theta + c, \quad y_0 = c - r_0 \sin\theta. \tag{4}$$

Equation (2) can be written as

$$(c + r_1 \sin\theta)^{\kappa_1/\kappa_0} (c - r_0 \sin\theta)^{\kappa_0/\kappa_1} \left(\frac{(r_1 + r_0)^2 \cos^2\theta + [2c + (r_1 - r_0)\sin\theta]^2}{(r_1 + r_0)^2} \right) = k^2.$$

Equation (1) requires that $\kappa_1 r_1 = \kappa_0 r_0$. Therefore the polar equation of motion for the vortex at (r_0, θ) is

$$(c + \beta^{-1} r_0 \sin\theta)^{\beta} (c - r_0 \sin\theta)^{1/\beta} \{r_0^2(\beta^{-1}+1)^2 \cos^2\theta + [2c + r_0(\beta^{-1}-1)\sin\theta]^2\} = r_0^2(\beta^{-1}+1)^2 k^2, \tag{5}$$

where $\kappa_1/\kappa_0 = \beta$ ($\beta > 0$). The vortex pairs must always pass one another at some time, i.e. there is always a solution of this equation for $\theta = \frac{1}{2}\pi$. However, for the paths of the vortex pairs to be closed curves, the equation must also have a solution for $\theta = 0$ for which the angular velocity of the motion is non-zero.

From (5) when $\theta = 0$

$$c^{\beta+1/\beta}[r_0^2(\beta^{-1}+1)^2 + 4c^2] = r_0^2(\beta^{-1}+1)^2 k^2,$$

$$r_0^2 = \frac{4c^{2+\beta+1/\beta}}{(\beta^{-1}+1)^2 (k^2 - c^{\beta+1/\beta})}.$$

This equation has real roots for

$$k^2 > c^{\beta+1/\beta}. \tag{6}$$

When $k^2 = c^{\beta+1/\beta}$, $r_0 \to \infty$. From (4) when $\theta = 0$

$$dy_0/dt = -r_0 d\theta/dt.$$

Equations (3) can be written as

$$\frac{dy_0}{dt} = \frac{-\kappa_1}{2\pi r_0(\beta^{-1}+1)}\left[1-\left(1+\frac{4c^2}{r_0^2(\beta^{-1}+1)^2}\right)^{-1}\right],$$

$$\frac{d\theta}{dt} = \frac{\beta\kappa_0}{2\pi r_0^2(\beta^{-1}+1)}\left[1-\left(1+\frac{4c^2}{r_0^2(\beta^{-1}+1)^2}\right)^{-1}\right].$$

Therefore, in this position ($\theta = 0$), $d\theta/dt$ is non-zero unless $r_0 \to \infty$.

The path of the vortex at (r_1, θ) is given by

$$(c+r_1\sin\theta)^\beta (c-\beta r_1\sin\theta)^{1/\beta}\{r_1^2(1+\beta)^2\cos^2\theta + [2c+r_1(1-\beta)\sin\theta]^2\} = r_1^2(1+\beta)^2k^2. \tag{7}$$

Similar analysis to that given for the vortex at (r_0, θ) again leads to equation (6) for the condition for periodic motion.

From (5) and (7), it can be seen that the closed curve will be symmetric about $\theta = \frac{1}{2}\pi$. The condition that the paths are closed curves is the condition that the motion is periodic, and it can be seen that the paths followed by the vortices are determined once their initial configuration is decided.

The vortices are moving about the point on the line joining them at $y = \bar{y} = c$, which is moving with a velocity $d\bar{x}/dt$ given by

$$(\kappa_1+\kappa_0)\frac{d\bar{x}}{dt} = \kappa_0\frac{dx_0}{dt} + \kappa_1\frac{dx_1}{dt}. \tag{8}$$

The period of the cycle is identical for the two vortices, the stronger moving on a shorter path inside that of the weaker. It can now be seen that the motion of each vortex pair is generally a cyclic motion similar to the threading motion of Helmholtz rings (Batchelor 1970).

When the vortices have the same strength, they move on identical paths about the midpoint of the line joining them. The equation of the path is

$$x^2y^2 + (k^2+c^2)y^2 + (k^2-c^2)x^2 - c^4 = 0$$

and (1) becomes $\bar{y} = c = \frac{1}{2}(y_1+y_0)$.

The condition for periodic motion is

$$k^2 > c^2. \tag{9}$$

When the condition (6) is not fulfilled, then the motion is neither cyclic nor repeated. However, since there must always be a configuration (past or future) when the vortices pass one another, condition (6) can be interpreted in terms of a critical ratio of the breadths of the vortex pairs.

Thus, writing $y_1 = Y_1$ and $y_0 = Y_0$ when $x_1 = x_0$, equations (1) and (2) become

$$(Y_0+\beta Y_1)/(1+\beta) = c \tag{10a}$$

and

$$Y_1^\beta Y_0^{1/\beta}\left(\frac{(Y_1+Y_0)^2}{(Y_1-Y_0)^2}\right) = k^2. \tag{10b}$$

Consider for the moment $\beta = 1$; then (9) requires

$$Y_1 Y_0 \left(\frac{Y_1+Y_0}{Y_1-Y_0}\right)^2 > \tfrac{1}{4}(Y_1+Y_0)^2,$$

$$(Y_1/Y_0)^2 - 6Y_1/Y_0 + 1 < 0,$$

$$Y_1/Y_0 < 3+2\sqrt{2}, \tag{11}$$

i.e. $Y_1/Y_0 < 5{\cdot}8282$ for periodic motion.

This is the condition obtained by Love, who considered this motion of vortices of equal strength. As he showed, the motion is periodic if, at the instant when one pair passes through the other, the ratio of the breadths is as given in (11). However, when $Y_1/Y_0 = 3+2\sqrt{2}$, then the smaller pair shoots ahead, and the larger pair does not catch it but contracts until both have the same breadth at $Y_1 = Y_0 = c$ and are an infinite distance apart. (Obviously, if the initial configuration is $\beta = 1, y_1 = y_0$, then no vertical motion ever occurs.) When $Y_1/Y_0 > 3+2\sqrt{2}$, the smaller pair moves ahead and widens to a constant breadth while the wider pair contracts, neither reaching the position $y = c$. Again they are ultimately an infinite distance apart.

Such a condition also exists when the vortices have different strengths. Equations (6) and (10) give

$$Y_1^{\beta} Y_0^{1/\beta} \left(\frac{Y_1+Y_0}{Y_1-Y_0}\right)^2 > \left(\frac{Y_0+\beta Y_1}{1+\beta}\right)^{\beta+1/\beta}, \tag{12a}$$

$$\left(\frac{1+\beta Y_1/Y_0}{1+\beta}\right)^{\beta+1/\beta} - \left(\frac{Y_1}{Y_0}\right)^{\beta}\left(\frac{1+Y_1/Y_0}{1-Y_1/Y_0}\right)^2 < 0. \tag{12b}$$

It should be noted that (10) are unchanged if β is replaced by $1/\beta$ and Y_1/Y_0 replaced by Y_0/Y_1; hence in evaluating (12) only values of $Y_1/Y_0 \geqslant 1$ need be considered. Let

$$f(\beta) = \left(\frac{1+\beta Y_1/Y_0}{1+\beta}\right)^{\beta+1/\beta} - \left(\frac{Y_1}{Y_0}\right)^{\beta}\left(\frac{1+Y_1/Y_0}{1-Y_1/Y_0}\right)^2.$$

Hence, from (12), the condition for a closed curve is $f(\beta) < 0$. Let $Y_1/Y_0 = 1+\epsilon$, where $\epsilon \geqslant 0$. Then

$$f(\beta) = \left(1+\frac{\beta\epsilon}{1+\beta}\right)^{\beta+1/\beta} - (1+\epsilon)^{\beta}\left(1+\frac{2}{\epsilon}\right)^2. \tag{13}$$

It can be shown from (13) that for all β

$$f(\beta) \to \begin{cases} -\infty & \text{as} \quad \epsilon \to 0, \\ \infty & \text{as} \quad \epsilon \to \infty. \end{cases}$$

Thus a critical value of Y_1/Y_0 as discussed for $\beta = 1$ exists for all β. As β is increased, this critical ratio is increased. However, as β is decreased ($\beta \ll 1$), there is a limiting value of Y_1/Y_0 below which the vortices are always locked in cyclic motion.

For $\beta \ll 1$, equation (13) becomes

$$f(\beta) = e^{\epsilon} - (1+\epsilon)^{\beta}(1+2/\epsilon)^2,$$

and as $\beta \to 0$,

$$f(\beta) \to f(0) = e^{\epsilon} - (1+2/\epsilon)^2. \tag{14}$$

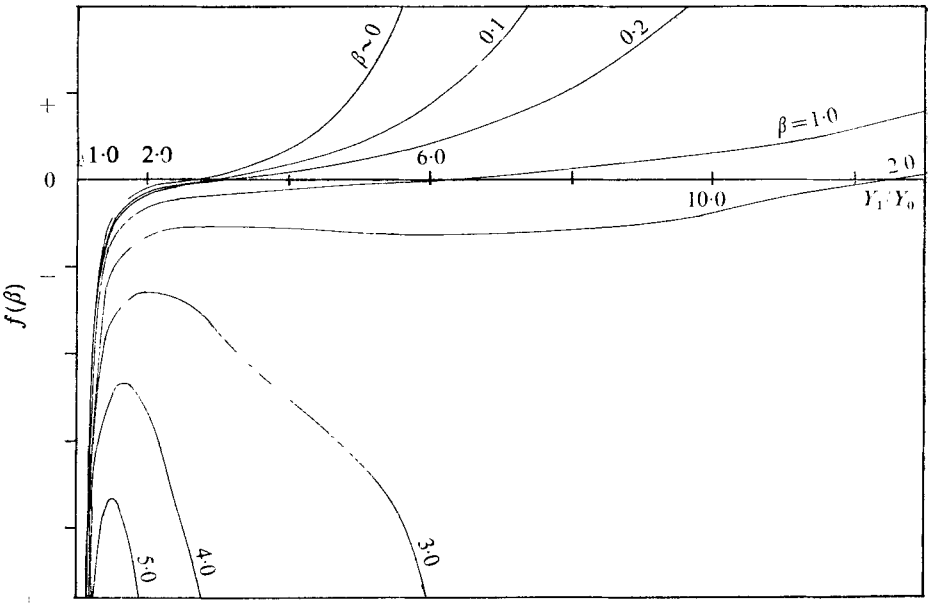

FIGURE 3. Curves showing some critical values of Y_1/Y_0 for cyclic motion ($f(\beta) < 0$) or non-cyclic motion ($f(\beta) > 0$).

This is the limiting curve and $f(0)$ changes sign when

$$\epsilon = 2\log_e(1+2/\epsilon).$$

This gives $$\lim (Y_1/Y_0) = 2{\cdot}61293 \quad \text{(to 5 decimal places)}. \tag{15}$$

For any value of Y_1/Y_0 less than this, the vortex pairs are locked in cyclic motion whatever their relative strengths.

Figure 3 shows $f(\beta)$ plotted against Y_1/Y_0 for several values of β. $f(\beta) < 0$ indicates the configurations for which periodic motion occurs. The critical value of Y_1/Y_0 for values of $\beta > 2$ is not shown; it becomes very large, e.g. when $\beta = 4, Y_1/Y_0 < 45$ gives periodic motion. It can also be seen that for $\beta \neq 1$ the situation arises where, for a particular value of Y_1/Y_0, the vortices are locked in cyclic motion if the weaker pair are the closer pair ($\beta > 1$), whilst they are not in cyclic motion if the stronger pair are closer together ($\beta < 1$).

The paths of the vortices were also computed. The starting configuration as shown in figure 1 was specified and also the relative strengths of the vortices. The induced velocity of one vortex due to the other three was calculated for each vortex in turn. From (3)

$$u_{ij} = \sum_{\substack{1 \\ k \neq i}}^{4} \frac{-\kappa_k(y_{ij}-y_{kj})}{(y_{ij}-y_{kj})^2+(x_{ij}-x_{kj})^2} \tag{16a}$$

and

$$v_{ij} = \sum_{\substack{1 \\ k \neq i}}^{4} \frac{\kappa_k(x_{ij}-x_{kj})}{(y_{ij}-y_{kj})^2+(x_{ij}-x_{kj})^2}. \tag{16b}$$

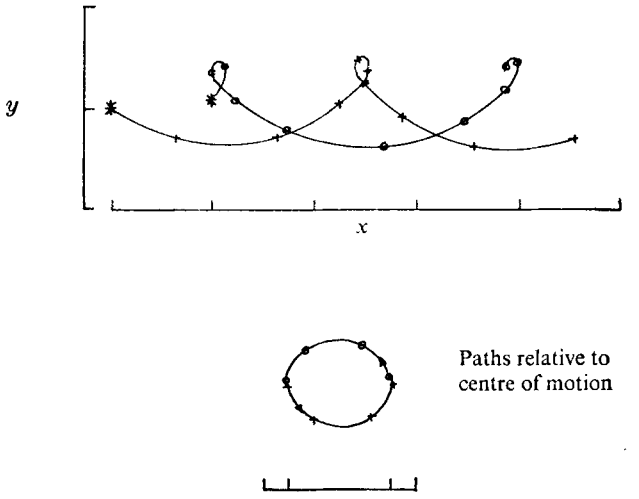

FIGURE 4. Typical cyclic paths of two identical vortex half-pairs ($\beta = 0$). ○, +, equal time intervals; *, initial positions.

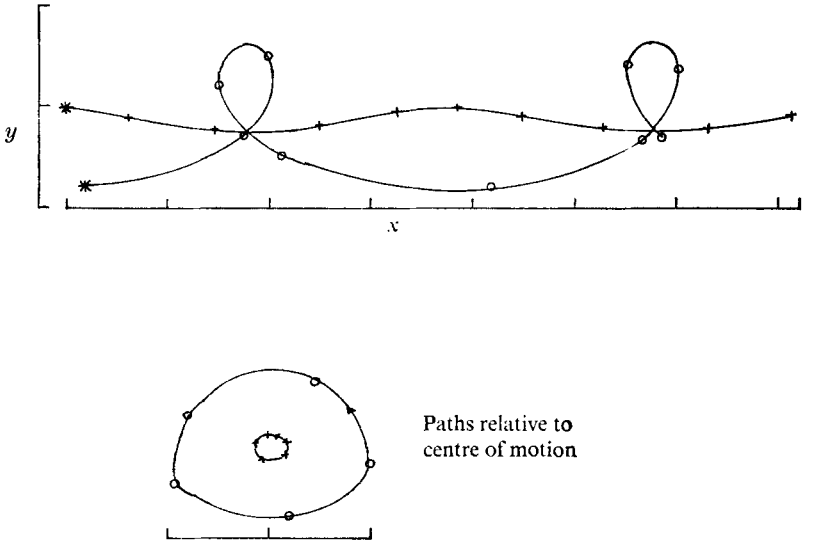

FIGURE 5. Typical cyclic paths of two vortex half-pairs with $\beta = 6$. Symbols as in figure 4.

New positions were then computed for each vortex:

$$\mathbf{x}_{i\,j+1} = \mathbf{x}_{ij} + \mathbf{u}_{ij}\Delta t, \tag{17}$$

where $\mathbf{x}_{ij} = (x_{ij}, y_{ij})$ is the jth position of ith vortex, $\mathbf{u}_{ij} = (u_{ij}, v_{ij})$ is the corresponding velocity and κ_i is the strength of ith vortex. The small time step Δt was based on checks during the running of the program on the magnitude of the acceleration and also on the angle turned through by the velocity vector.

Some examples of the motion of the vortex half-pairs are given in figures 4 and 5. As shown previously, the paths followed by the vortices are determined

solely by their initial positions. The typical threading motion with $\beta = 1$ is shown in figure 4. The same path relative to the midpoint of the line joining the vortices is shown. Markers showing equal intervals of time indicate the relative time spent in each part of the motion. It can be seen that, during the slowest part of the cycle, the vortices loop backwards in their paths.

If the vortices are initially set much closer together, this backwards looping becomes more marked, the net movement in the x direction being small. When the vortices are set further apart, the path shapes are considerably elongated in the x direction.

In the situation shown in figure 4, $Y_1/Y_0 = 2{\cdot}4$ (when the vortices are vertically in line), which may be compared with equation (11). It can be shown that, for these vortices not to be 'locked' in cyclic motion, the initial separation in the x direction must be increased by a factor of 44.

The form of motion when the vortices have different strengths is shown in figure 5. The paths of the vortex half-pairs are now not the same, but as before, a larger initial separation elongates the paths in the x direction.

The motion of these vortices is again completely determined by the initial configuration. In order to consider further the motion of these discrete vortex pairs, the motion of two vortices moving initially in opposite directions was also investigated. This corresponds to negative values of β.

In the particular case $\beta = -1$, (1) and (2) become

$$y_1 - y_0 = \text{constant}, \tag{18}$$

$$\frac{1}{y_1 y_0}\left(\frac{(x_1-x_0)^2+(y_1+y_0)^2}{(x_1-x_0)^2+(y_1-y_0)^2}\right) = k^2. \tag{19}$$

When $y_1 = y_0$ initially, this relationship is maintained during all subsequent motion:

$$y_1 = y_0 = y, \quad dy_1/dt = dy_0/dt.$$

From (3)
$$dx_1/dt = -dx_0/dt.$$

Hence $x_1 = -x_0 = x$ in all subsequent motion and from (19)

$$y^{-2} + x^{-2} = k^2. \tag{20}$$

This is the well-known equation (Lamb, art. 155) for the paths of the vortices, where as they approach closely they move away from the boundary and $y \to \infty$. When $y_1 \neq y_0$, (1) continues to hold and the paths are of similar form to (20). Typical paths are shown in figure 6.

When the vortices are of opposite sign and different strengths, they do not remain together but after some deviation from their original paths pass one another and continue moving in opposite directions. The exact form of the paths followed depends only on the relative strength of the vortices and the value of the constant in (1). Some typical paths are shown in figure 7.

This type of interaction between vortices of opposite sign thus never involves any pairing or periodic behaviour of the vortices. The paths are again determinable once initial conditions are specified.

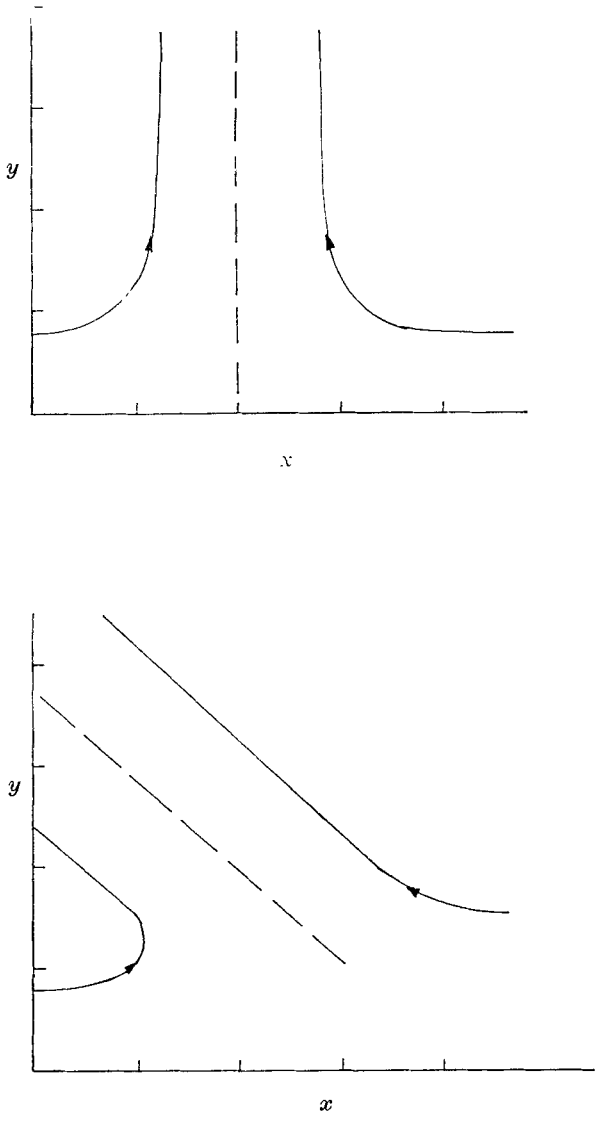

FIGURE 6. Typical paths of two identical vortex half-pairs of opposite sign ($\beta = -1$).

The motion of three vortex half-pairs was also considered. Similar relationships to (1) and (2) hold. Thus, for three vortices of the same sign, the motion is again periodic and determinable from the initial conditions. If just two of the vortices have the same sign, then condition (6) is applicable to them and the approach of the third vortex produces a combination of the previously described paths. Typical examples are shown in figures 8(*a*) and (*b*). When the two vortices of the same sign are not initially set in cyclic motion according to condition (6), then the approach of the third vortex can affect the motion such that cyclic motion results. This is shown in figure 8(*c*). This is the only case in this simple

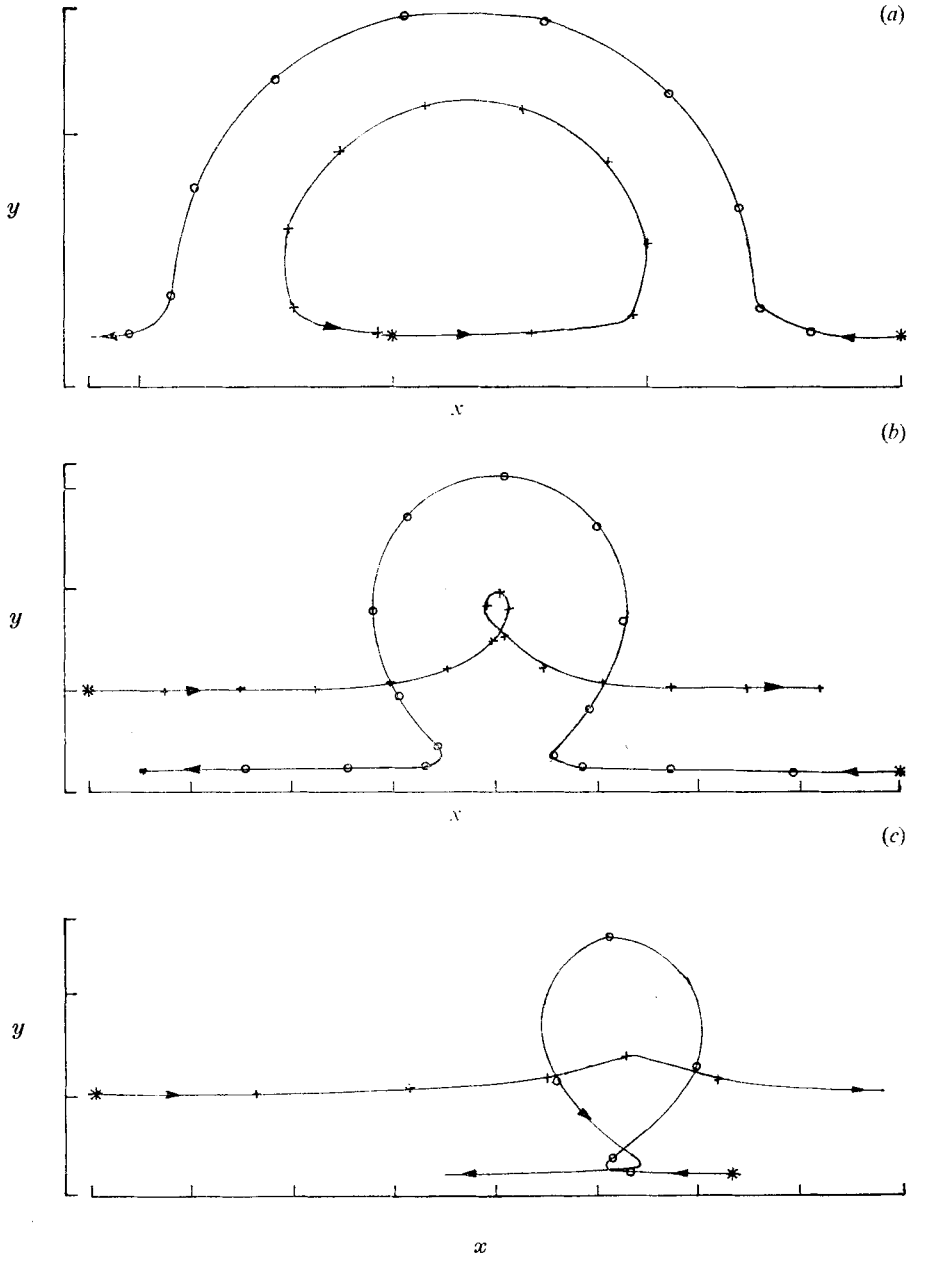

FIGURE 7. Typical paths of two vortex half-pairs of opposite sign. (*a*) $\beta = -1{\cdot}4$. (*b*) $\beta = -3$. (*c*) $\beta = -6$. Symbols as in figure 4.

modelling with discrete vortex pairs in which periodic motion evolves from a non-cyclic situation. A third vortex of opposite sign can thus act as a 'catalyst' to give cyclic motion. However, this is not obviously applicable to the coalescence of vortices observed in shear layers since those vortices essentially have the same sign.

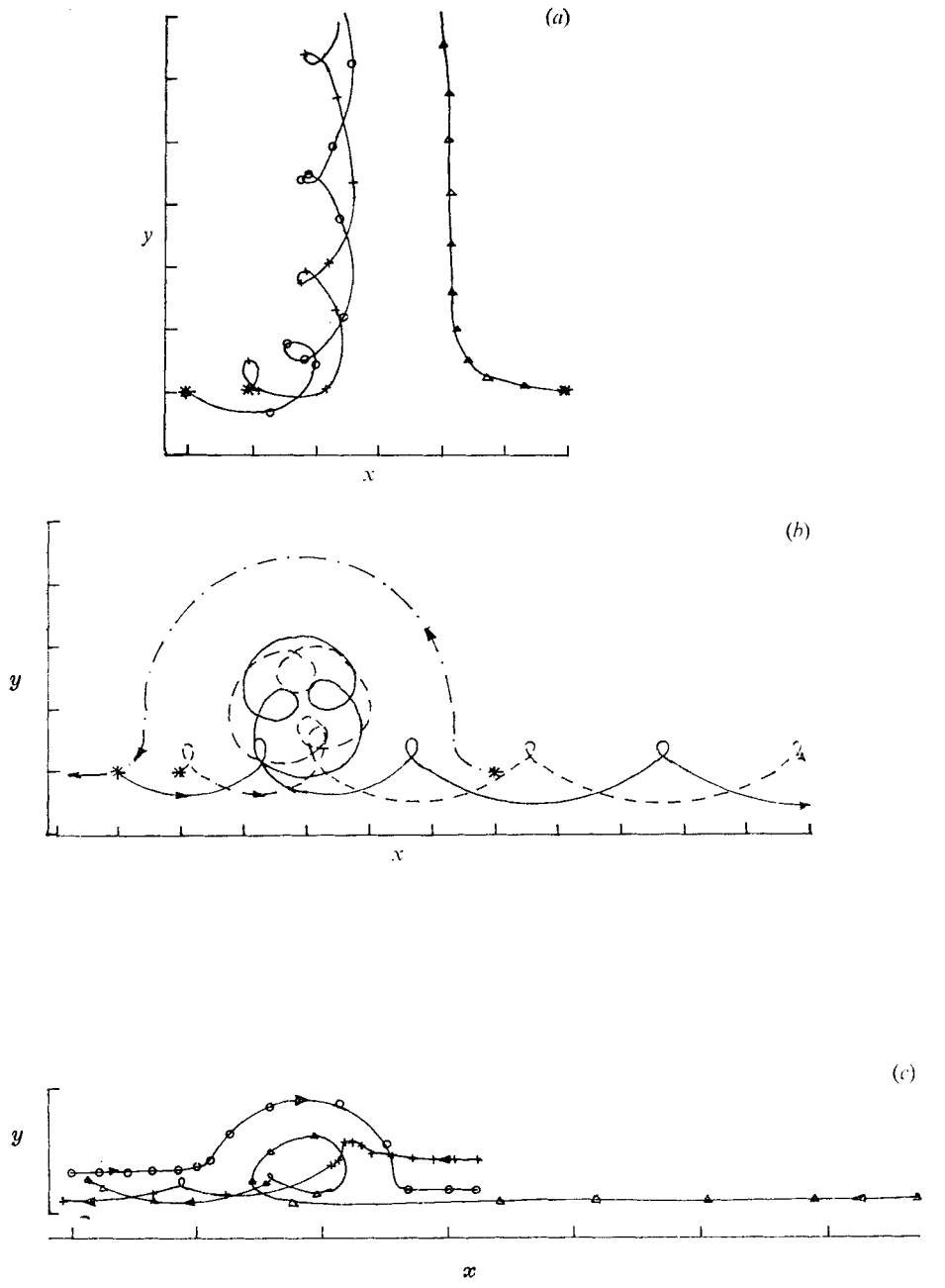

FIGURE 8. The paths of three vortex half-pairs showing the motion of two half-pairs in the presence of a third vortex of opposite sign. (*a*) —○—, —┼—, $\kappa = 1$; —△—, $\kappa = -2$. (*b*) ——, – – –, $\kappa = 1$; —·—, $\kappa = -1$. (*c*) An example of 'catalytic pairing': —△—, —┼—, $\kappa = -1$; —○—, $\kappa = 1$.

It thus appears to us, despite Winant & Browand's apparently convincing statements to the contrary, that elementary isolated line vortices cannot adequately represent the vortex pairing action observed in shear layers. The cyclic motion described here is essentially non-evolutionary; there is no tendency for vortices to coalesce. Such coalescence depends on finer details in the shear layer. A modelling of that detailed structure is attempted in the next section, where the shear layer is represented by a continuous array of elementary line vortices.

3. The discrete-vortex modelling of a two-dimensional shear layer

The vortex sheet

A simple extension of the previous model to form a vortex sheet of finite length has immediate difficulties: the ends of the sheet roll up. This gradually distorts the whole layer and the number of elements required to give a short undisturbed region in the middle becomes uneconomically high.

This problem was overcome here by repetition of elements in a cyclic array to form an infinite shear layer. The number of vortices and their initial distribution within a cycle can be specified and the induced velocities due to the whole sheet calculated. The complex potential w of an infinite row of equidistant vortices of equal strength κ and spacing a is

$$w(z) = \frac{i\kappa}{2\pi}\log_e \sin\frac{\pi z}{a}$$

(Lamb 1924, art. 156), giving

$$u(x,y) = \frac{-\kappa \sinh 2\pi y/a}{2a\,(\cosh 2\pi y/a - \cos 2\pi x/a)},$$

$$v(x,y) = \frac{\kappa \sin 2\pi y/a}{2a\,(\cosh 2\pi y/a - \cos 2\pi x/a)}.$$

We write these velocities in the notation of (16) and calculate the induced velocities of all n vortices in the 'cycle' length a:

$$u_{ij} = \sum_{\substack{k=1\\k\neq i}}^{n} \frac{-\kappa_k \sinh 2\pi a^{-1}(y_{ij}-y_{kj})}{2a\,[\cosh 2\pi a^{-1}(y_{ij}-y_{kj}) - \cos 2\pi a^{-1}(x_{ij}-x_{kj})]}, \tag{21}$$

$$v_{ij} = \sum_{\substack{k=1\\k\neq i}}^{n} \frac{\kappa_k \sin 2\pi a^{-1}(x_{ij}-x_{kj})}{2a\,[\cosh 2\pi a^{-1}(y_{ij}-y_{kj}) - \cos 2\pi a^{-1}(x_{ij}-x_{kj})]}. \tag{22}$$

These are evaluated and substituted in (17) to calculate the motion. A non-dimensional time parameter T may be defined here. The n vortices distributed along a wavelength λ cause a net velocity discontinuity ΔU across the sheet which is given by

$$\Delta U\lambda = n\kappa. \tag{23}$$

Define

$$T = \frac{t\Delta U}{2\lambda} = \frac{n\kappa}{2\lambda^2}t. \tag{24}$$

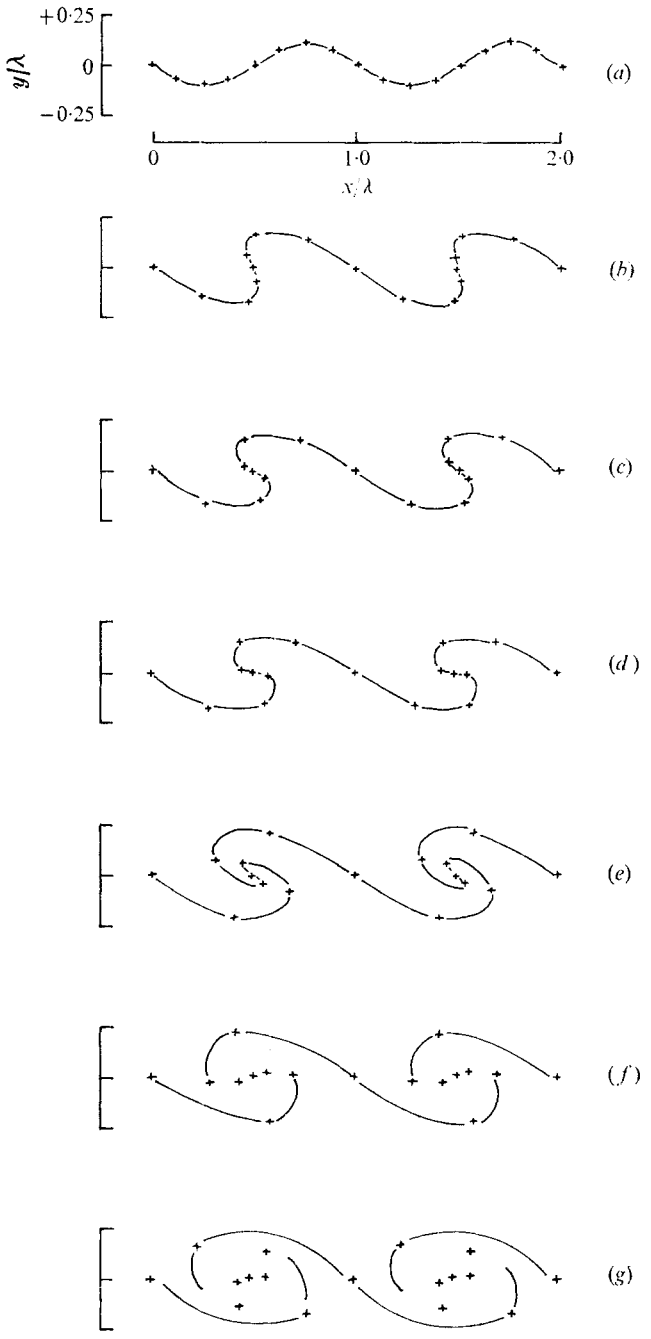

FIGURE 9. The development of a vortex sheet represented by discrete vortex elements. (*a*) $T = 0$. (*b*) $T = 0{\cdot}30$. (*c*) $T = 0{\cdot}35$. (*d*) $T = 0{\cdot}38$. (*e*) $T = 0{\cdot}53$. (*f*) $T = 0{\cdot}69$. (*g*) $T = 0{\cdot}92$.

This representation of a vortex sheet was first considered by Rosenhead (1932), who specified the repetition of a single wavelength of four, eight or twelve vortices distributed evenly along a sine wave. Rosenhead took very large time steps in his 'hand' calculations and observed that the surface tended at first to roll over itself like a breaking wave and then proceeded smoothly to roll up to a concentration of vorticity.

The object here is to specify several wavelengths and to observe any interaction between the rolled-up structures. A sinusoidal distribution of 8 vortices per wavelength and their subsequent motion are shown in figure 9. The rolling up of the sheet proceeds smoothly. The overall time for roll-up and the shape are in agreement with those found by Rosenhead although the time step taken here is very much smaller ($\Delta T = 0{\cdot}001$). When non-uniformities were introduced into the defined cycle, the layer rolled up in a non-uniform way. However, this had no observable effect on the larger-scale motion which is our particular concern here.

Obviously there is too little definition in the sheet shown in figure 9, so the number of vortices in the representation was increased. With 24 vortices the situation was quite chaotic, essentially because of the critical closeness of vortex elements, which allows the motion to be dominated by the more unstable smaller scales. However, the overall time taken to roll up was unaffected by this. This behaviour has been observed by several authors: Hama & Burke (1960) also repeated Rosenhead's calculations (with $\Delta T = 0{\cdot}025$) and suggested that, by taking large time steps, Rosenhead had eliminated the effect of the small-scale motion. Later, Moore (1971) conclusively showed that the contorted roll-up was not due to inaccuracies in the computation and that increasing the number of vortices worsens the situation. A finer digitization represents the pathologically unstable vortex sheet more accurately. The basic model is at fault.

Chorin & Bernard (1972) felt that it is the high induced velocities which occur when two vortices come close together that invalidates the model. They suggested the introduction of a finite-radius core to the vortices. The equation for the stream function of a single vortex then becomes

$$\psi = \begin{cases} (\kappa/2\pi)\log_e r & \text{for} \quad r \geqslant \sigma, \\ \frac{1}{2}\kappa r/\sigma & \text{for} \quad r < \sigma, \end{cases} \tag{25}$$

where σ is a small cut-off radius. Chorin & Bernard suggested that this cut-off is analogous to the introduction of a small viscosity which allows the vorticity in a line vortex to diffuse. The effect is not cumulative; the vorticity is spread a little way only. They were able to show that for $\sigma \neq 0$ the roll-up proceeded smoothly, and the results were independent of σ for σ small.

In order to give the shear layer increased definition and also to reduce the irrelevant small-scale rippling, the layer was given a finite thickness. Several rows of vortices (12 per wavelength row) were specified, each identical, but with a small separation between the rows. A cut-off was applied to the velocity induced by each vortex element. The radius σ for the cut-off was chosen as the smallest that had the necessary, in fact any, effect. It was then found that a smooth rolling-up of the layer could be achieved.

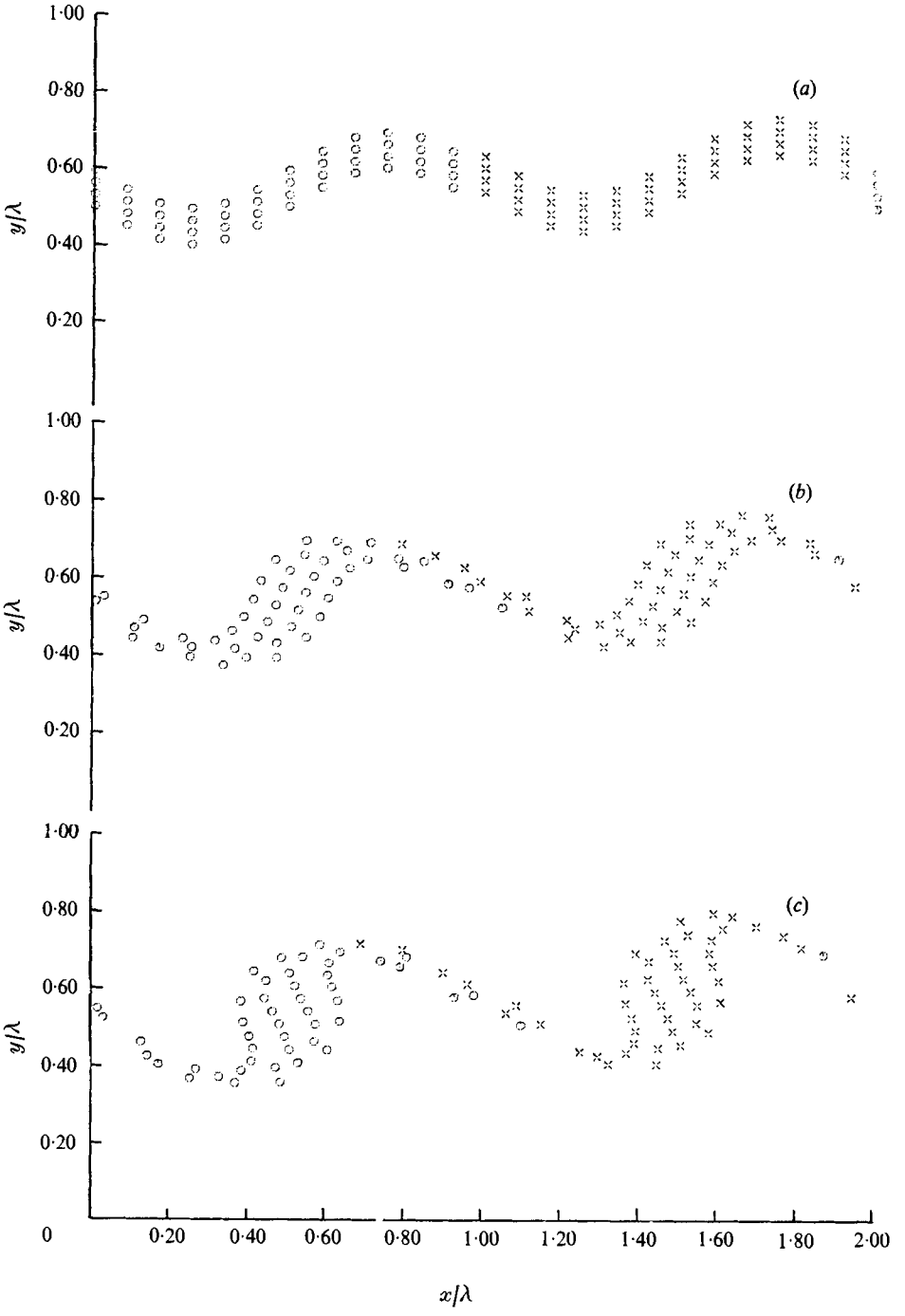

FIGURES 10 (*a–c*). For legend see page 580.

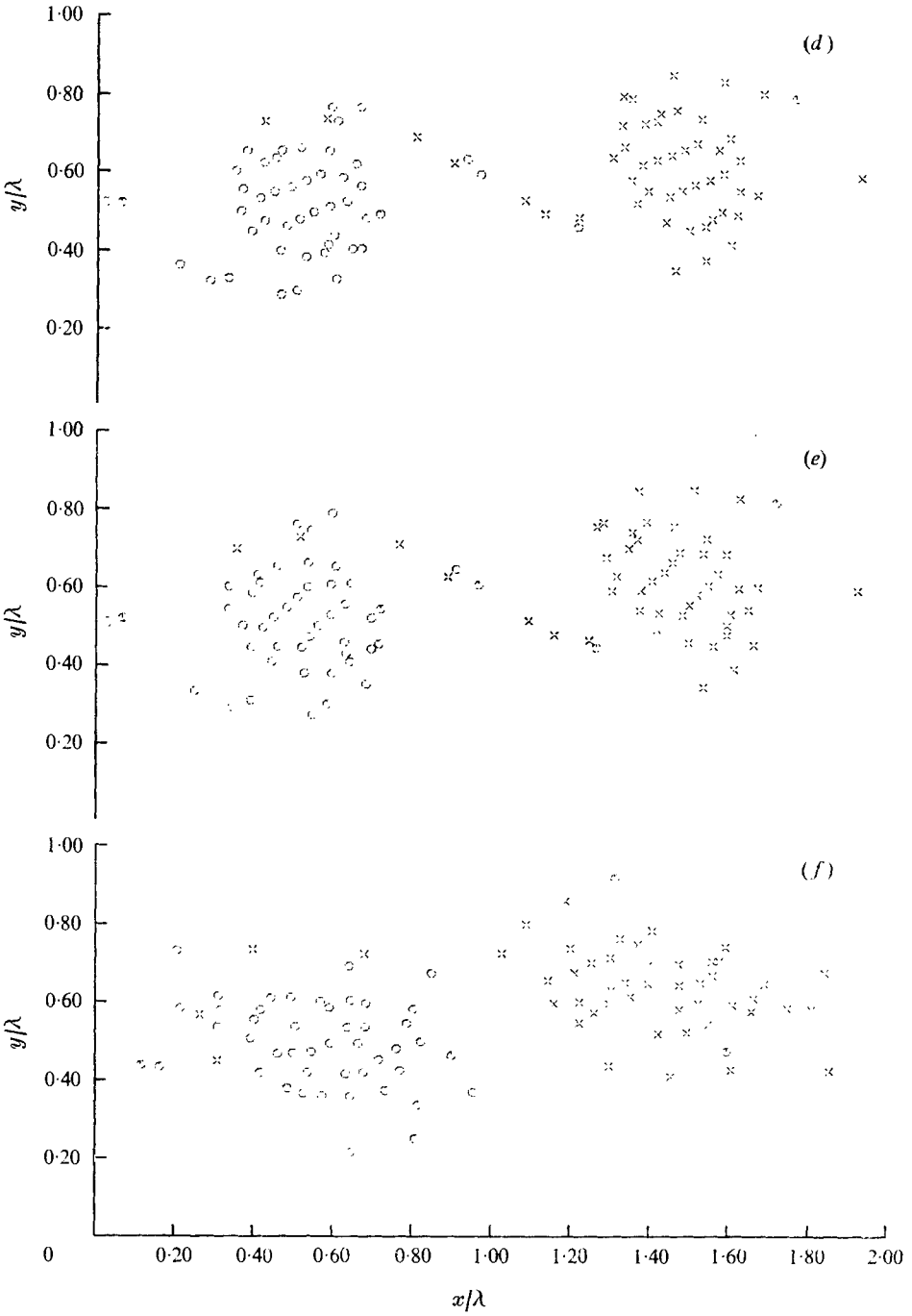

FIGURES 10 (*d–f*). For legend see page 580.

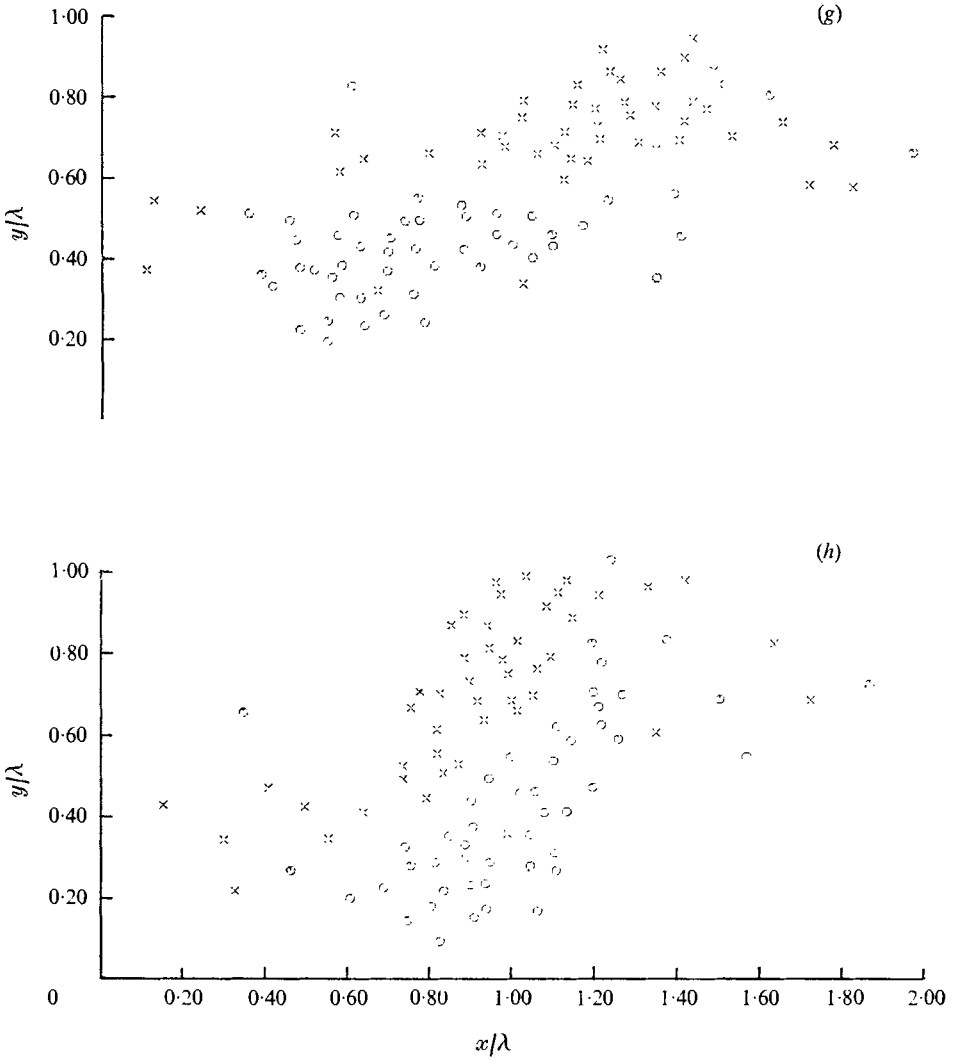

FIGURES 10 (*g*, *h*). For legend see page 580.

The shear layer of finite thickness

The typical starting configuration is shown in figure 10(*a*), for $T = 0$. The specified length for repetition contains 96 vortices arranged evenly in four rows along two sinusoidal wavelengths. The layer has a finite thickness Δ, and the second wavelength is offset vertically by a length δ. The two sections have the same wavelength λ and amplitude A.

The subsequent development of the layer is shown in figures 10(*b*)–(*j*). The values of the non-dimensional parameters are given in table 1, case 1. It can be seen that the sheet rolls up to form concentrations which rotate about their own axes and then about one another until they coalesce. A single structure is then formed which continues to rotate about its own axis. Interaction between these large structures is prevented in our model by the cyclic repetition condition.

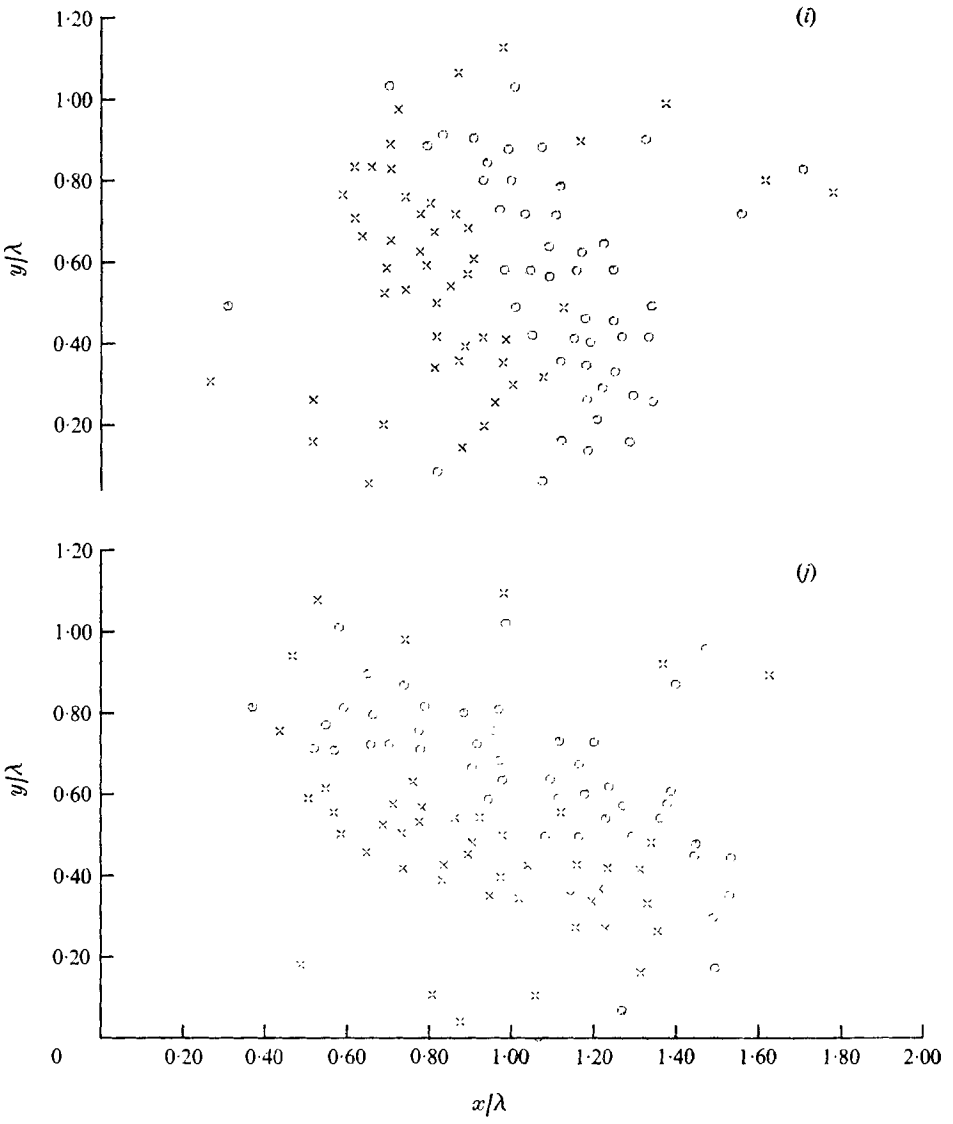

FIGURE 10. The development of a thick shear layer represented by discrete vortex elements (circles and crosses). (*a*) $T = 0$. (*b*) $T = 0{\cdot}264$. (*c*) $T = 0{\cdot}377$. (*d*) $T = 0{\cdot}603$. (*e*) $T = 0{\cdot}666$. (*f*) $T = 1{\cdot}043$. (*g*) $T = 1{\cdot}696$. (*h*) $T = 2{\cdot}111$. (*i*) $T = 2{\cdot}488$. (*j*) $T = 2{\cdot}840$.

During the initial stages of the rolling-up (up to $T = 1{\cdot}0$), the structure of the rolled-up sheet seems well defined. However, once the 'eddy' is well formed and begins to rotate, it loses this structure and remains a smeared-out concentration of vorticity. In order to discover the degree of definition in the initial structure, a vertical row of flow markers was incorporated. Two situations were considered. First, the markers were active vortices with equal strengths such that the overall strength of the wavelength was unaltered. In the second case, the markers were passive elements moving under the influence of the surrounding vortices only.

	Case	Δ/λ	A/λ	δ/λ
	1	0·0938	0·1	0·0375
Variation of Δ	2	0·15	0·1	0·0375
	3	0·25	0·1	0·0375
	4	0·4	0·1	0·0
	5	0·06	0·1	0·0
Variation of A	6	0·09375	0·05	0·0375
	7	0·09375	0·025	0·0
	8	0·09375	0·025	0·01
	9	0·09375	0·025	0·0375
	10	0·06	0·01	0·0
Variation of δ	11	0·09375	0·1	0·0025
	12	0·09375	0·1	0·01
	13	0·09375	0·1	0·01875
	14	0·09375	0·1	0·0755
	15	0·09375	0·1	0·11
	16	0·09375	0·1	0·25

TABLE 1. The variation of the parameters of the model of a thick shear layer

These are shown in figures 11 and 12. The active markers (figure 11) show smooth initial development but stretch out to form a single row of vortices: a vortex sheet which then exhibits instability. The passive markers (figure 12) simply rotate around their closest active neighbour. It can thus be seen, as expected, that our discrete model cannot represent fine-scale shear-layer structure; that fine-scale structure should therefore be ignored.

In this and subsequent cases the time step was larger ($\Delta T = 0{\cdot}0125$) than that used for the development of the computer program. This was desirable in order to reduce the computation time, and was found to have no significant effect. As previously discussed, it is necessary for each vortex to have a finite-radius core to reduce the high velocities of small-scale instabilities that would be induced on neighbouring vortex elements. The model core used here is that given by (25); the large-scale behaviour was not affected by the choice of core.

The thickness H of both the single structures and the overall layer can be estimated for the development shown in figure 10. There is an initial rapid growth as the layer rolls up, which then decreases as the vortex rotates about its own axis and is elongated in the direction of mean strain. The form of this growth is matched by that of the layer as a whole. However, as the vortices begin to move closer there is further rapid growth as coalescence takes place and the two vortices lose their separate identities. This growth is shown in figure 13. It can be seen that, as the larger eddy begins to rotate about its own axis, the width again decreases a little.

The growth of the width of the layer obviously depends on the initial configuration of the larger. This dependence was investigated by varying the parameters involved over the range indicated in table 1. The initial layer thickness was varied by increasing the separation between the rows of vortices or by increasing

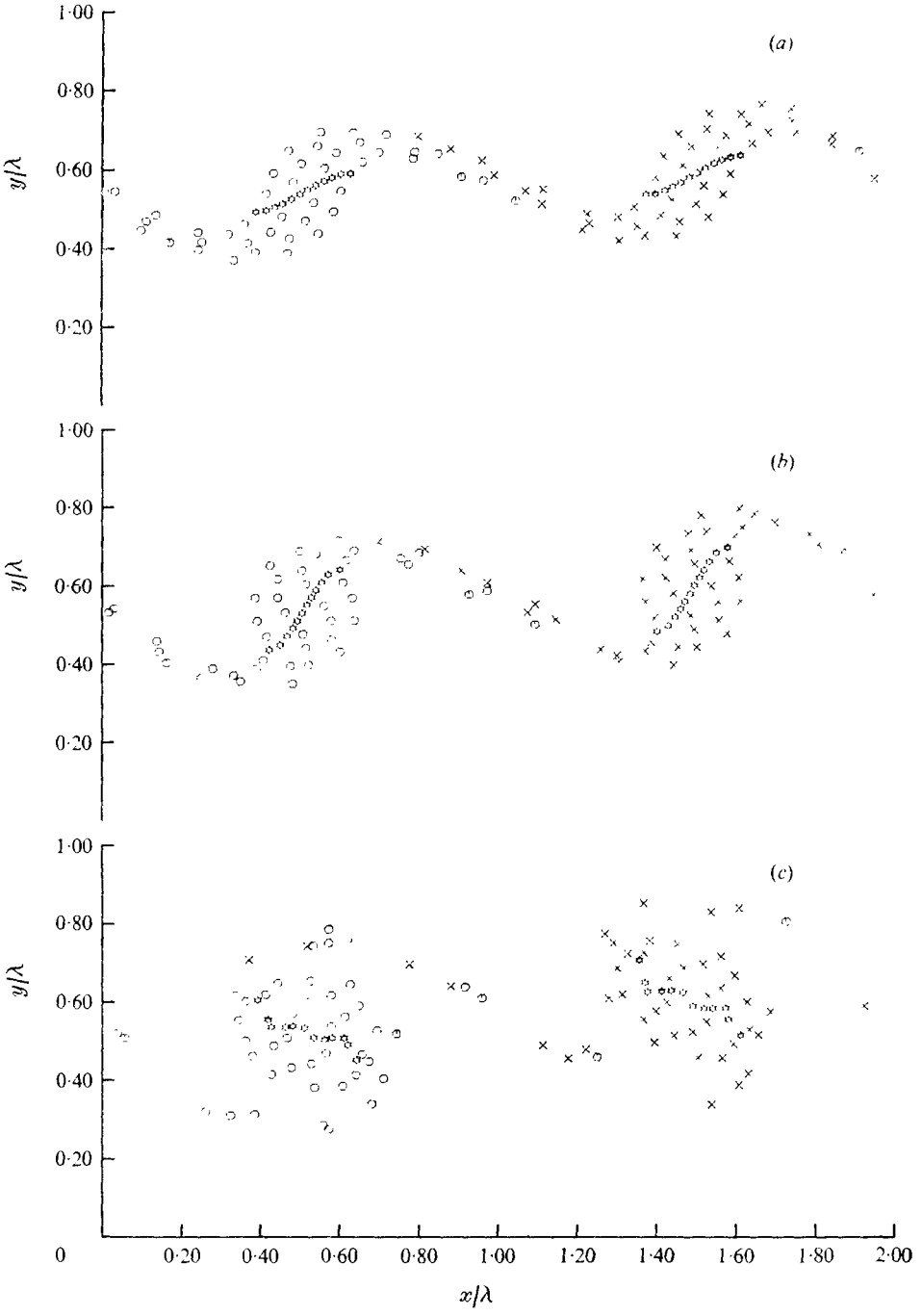

FIGURE 11. The development of the shear layer showing the motion of active flow markers. ○, ×, vortex elements; ☆, flow markers. (*a*) $T = 0{\cdot}264$. (*b*) $T = 0{\cdot}377$. (*c*) $T = 0{\cdot}666$.

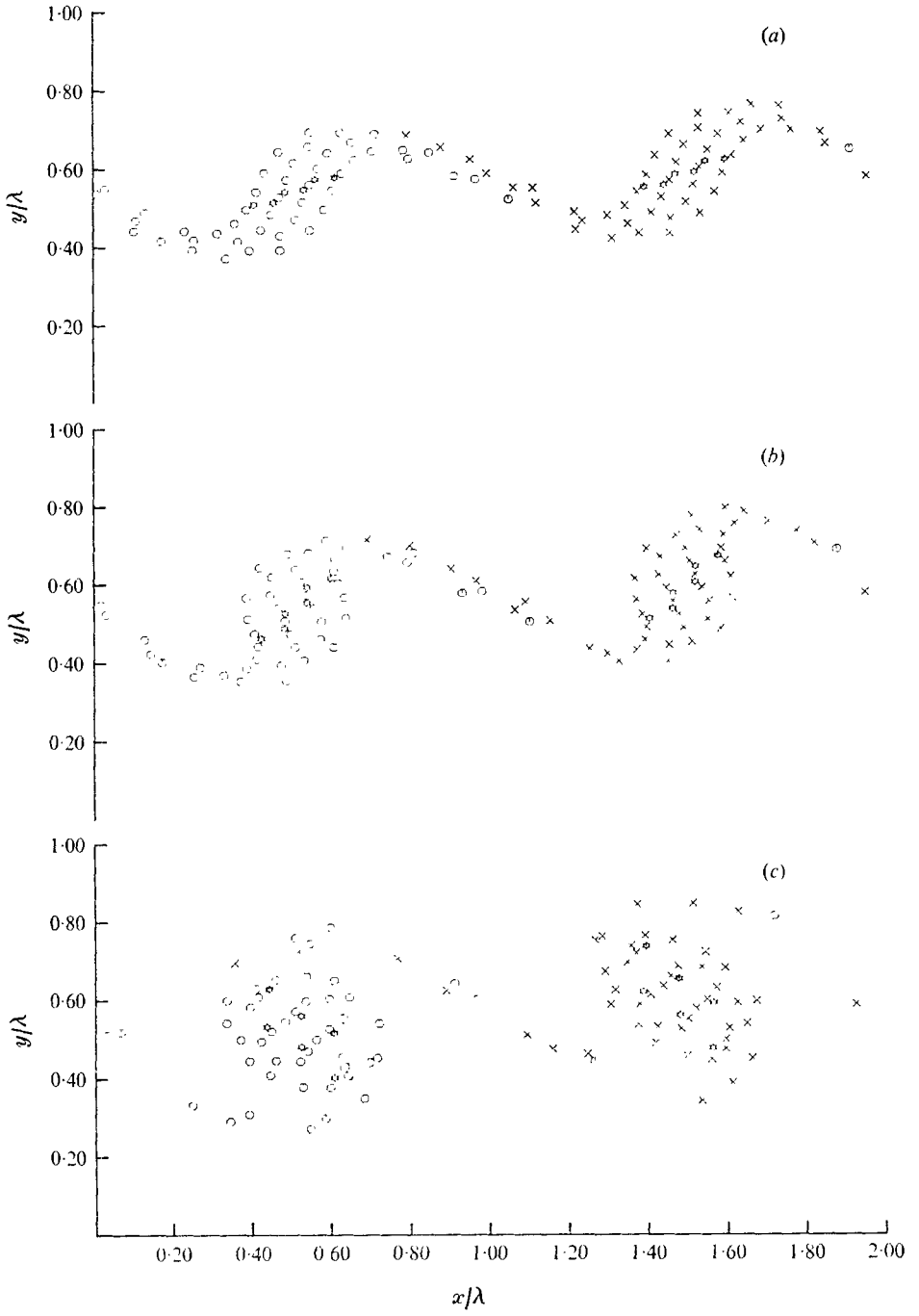

FIGURE 12. The development of the shear layer showing the motion of passive flow markers. O, ×, vortex elements; ☆, flow markers. (*a*) $T = 0{\cdot}264$. (*b*) $T = 0{\cdot}377$. (*c*) $T = 0{\cdot}666$.

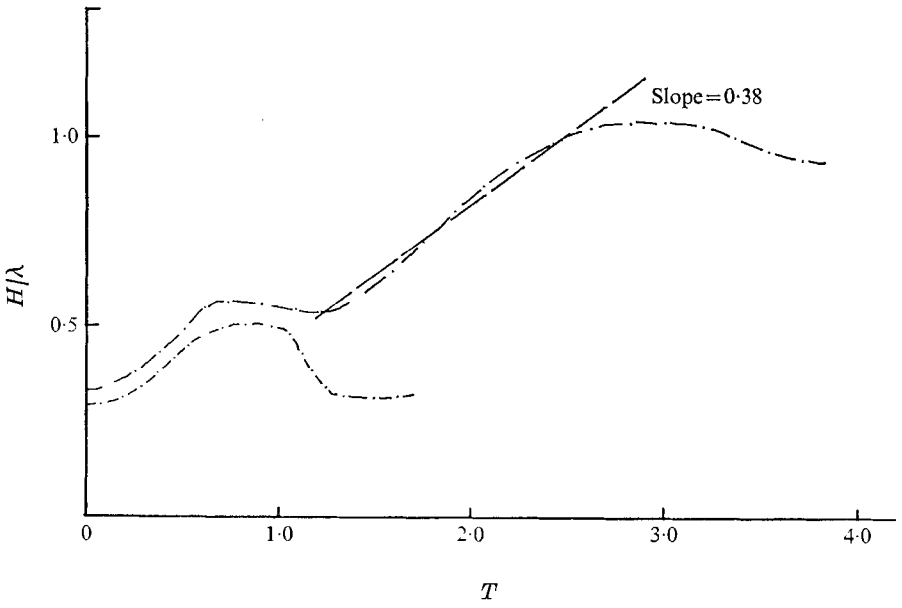

FIGURE 13. Typical growth of the width of a single structure and the overall shear layer. $A/\lambda = 0{\cdot}1$, $\Delta/\lambda = 0{\cdot}09375$, $\delta/\lambda = 0{\cdot}0375$.

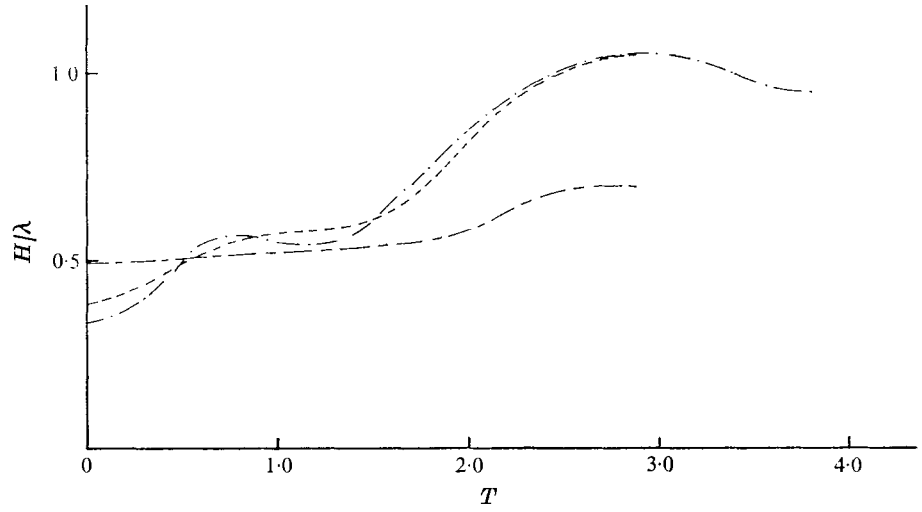

FIGURE 14. The effect of shear-layer thickness on the growth of the overall width of the layer. $A/\lambda = 0{\cdot}1$, $\delta/\lambda = 0{\cdot}0375$. —·—, $\Delta/\lambda = 0{\cdot}09375$; – – –, $\Delta/\lambda = 0{\cdot}15$; — – —, $\Delta/\lambda = 0{\cdot}25$.

the number of rows. As the thickness Δ is increased, there is a slower rate of rotation in the rolling-up of the layer. The increase in the width H is correspondingly slower as shown in figure 15. In the extreme case when $\Delta/\lambda = 0{\cdot}4$, there is no growth at all. The structures formed with increased Δ are longer and coalescence is therefore able to occur quicker as shown in figure 14. Case 3, where $\Delta/\lambda = 0{\cdot}25$, is seen to represent a limiting case in the form of the coalescence.

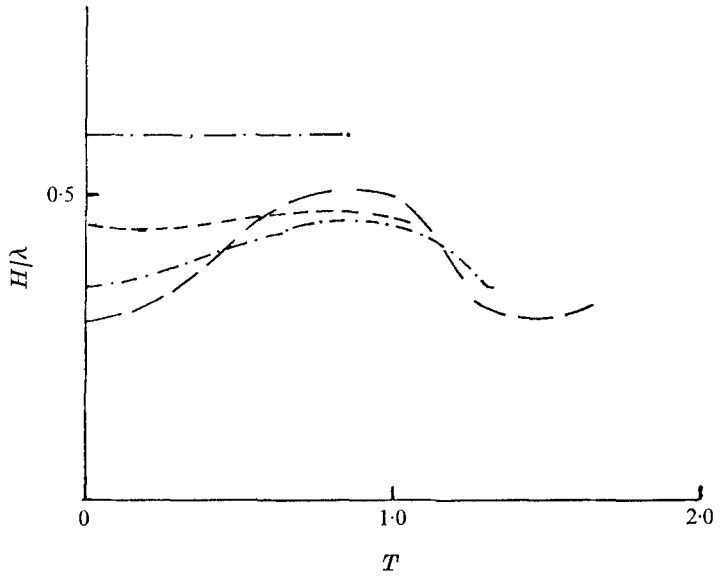

FIGURE 15. The effect of initial shear-layer thickness on the growth of the single structure. $A/\lambda = 0{\cdot}1$. — —, $\Delta/\lambda = 0{\cdot}09375$; —·—, $\Delta/\lambda = 0{\cdot}15$; – – –, $\Delta/\lambda = 0{\cdot}25$; —·—, $\Delta/\lambda = 0{\cdot}4$.

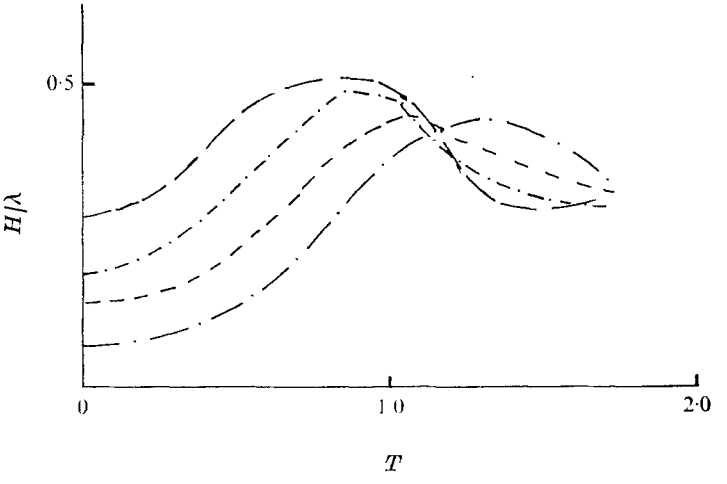

FIGURE 16. The effect of initial amplitude on the growth of the single structure. — —, $A/\lambda = 0{\cdot}1$, $\Delta/\lambda = 0{\cdot}09375$; –·–·–, $A/\lambda = 0{\cdot}05$, $\Delta/\lambda = 0\ 09375$; – – –, $A/\lambda = 0{\cdot}025$, $\Delta/\lambda = 0{\cdot}09375$; —·—, $A/\lambda = 0{\cdot}01$, $\Delta/\lambda = 0{\cdot}06$.

The final value of the width H is smaller than with an initially smaller thickness Δ. This appears to be due to the large streamwise length of the two vortex concentrations, which causes them to be too close together to rotate about one another. They coalesce under the shearing action of the layer. In case 4, where there was no initial growth, no recognizable vortex structure forms and the layer remains a single thick layer which could periodically thicken.

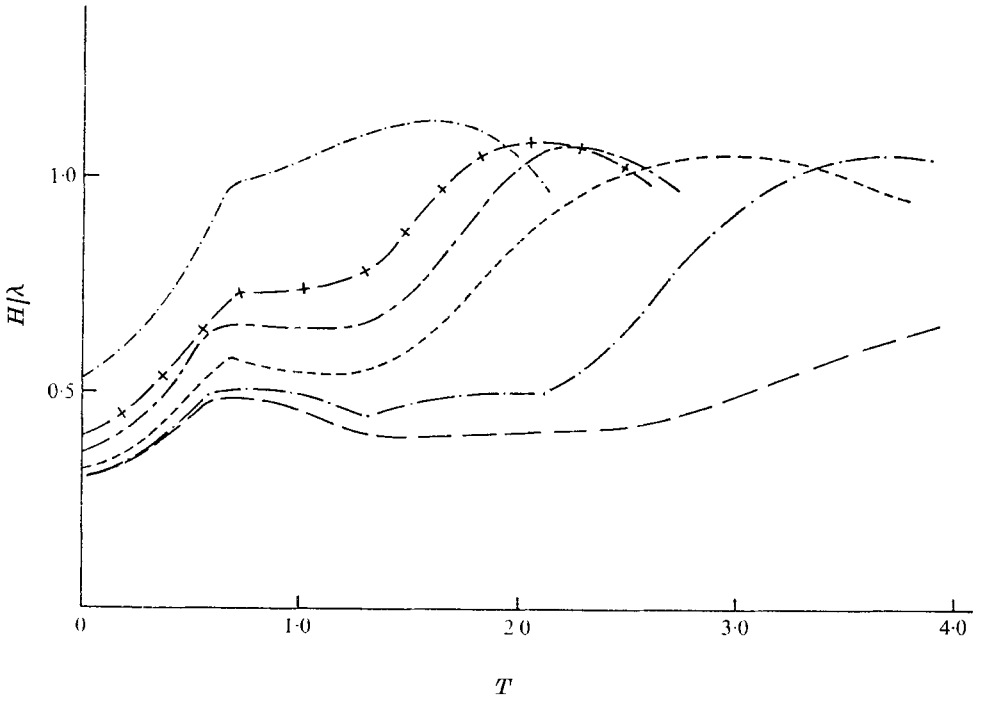

FIGURE 17. The effect of initial lateral spacing on the growth of the overall width of the layer. $A/\lambda = 0{\cdot}1$, $\Delta/\lambda = 0{\cdot}09375$. — —, $\delta/\lambda = 0{\cdot}0025$; —·—, $\delta/\lambda = 0{\cdot}1$; – – –, $\delta/\lambda = 0{\cdot}0375$; — – —, $\delta/\lambda = 0{\cdot}0755$; —+—, $\delta/\lambda = 0{\cdot}11$; -·-·-, $\delta/\lambda = 0{\cdot}25$.

When the amplitude of the initial wave form is decreased, the rate of rotation during the rolling-up of the layer is slower. The single structures are then well separated and do not form such elliptical shapes. The growth of the width of the single structures is shown in figure 16. It can be seen that the curves form a 'family' which reach their maxima later with decreasing initial amplitude.

For the values of δ/λ given in table 1, the initial rolling-up of the shear layer occurs as shown in figure 10, and the form does not change significantly with changes in this lateral irregularity δ. However, as δ is increased the coalescence occurs sooner. This is shown in figure 17, where the overall layer width follows that of the single structures for a shorter time.

In summary, the effects of the initial conditions are as follows.

(i) The initial shear-layer thickness governs the initial roll-up rate of the layer. It can also serve to inhibit the pairing process.

(ii) The time taken to reach the maximum rolled-up width is the same for all initial layer thicknesses (for the same initial amplitude).

(iii) The effect of decreasing the amplitude is to delay the rolling-up.

(iv) The time taken for coalescence is determined solely by the lateral irregularity δ.

(v) The process is always relatively abrupt, it simply takes longer to begin for smaller δ.

4. Discussion

The initial stages in the eddy development are essentially those common to aspects of nonlinear transition of laminar flows. Michalke (1963) has shown, using linear stability theory for a shear layer with a linear velocity profile, that maximum amplification of the disturbance occurs when the thickness ratio $\Delta/\lambda \simeq 0{\cdot}126$. The corresponding exponential growth rate is 0·2. A sinusoidal form of the shear layer occurs when the amplitude ratio A/λ reaches about 0·02. These values are within the ranges considered here. The initial exponential growth rate of case 2, (table 1) with $\Delta/\lambda = 0{\cdot}15$, is in agreement with these calculations, although the development is soon nonlinear because of the high amplitude ratio. The modelled shear layer is given a disturbance of finite amplitude, which is thus assumed feasible at the onset of nonlinearity. This is not directly relevant to the pairing process. It is, however, one way in which the eddies which form the large-scale structure could evolve. It is probably more realistic than an infinite array of single point vortices at the centres of vorticity of the coalescing structures. The paths followed by the vortices for that configuration are shown in figure 18. These paths are those of Winant & Browand's model and are continuously repeated. It can be seen that the two vortices are not locked together in cyclic motion, and cannot represent the pairing process.

In the model presented here, the structures in the specified length are repeated in a cyclic array to infinity. However, in the real turbulent flow, all parts of the layer would be at different stages of evolution, and it might be supposed that this would significantly affect the eddy development. Therefore a longer specified length of five wavelengths was considered. Two wavelengths were described as in figure 10 and the outer wavelengths consisted of smaller, differing amplitudes. It was found that the coalescence was substantially independent of the form of the surrounding wavelengths and it is thus probable that the interactions described here actually occur in a real growing shear layer.

Our model was extended to represent both the symmetric and antisymmetric development of a planar jet by specifying two parallel shear layers. The sinuous form of the jet observed by Rockwell & Niccolls (1972) can thus be modelled. (An example of this is given in figure 19.) They also observed at low Reynolds number a 'nascent coalescence' where embryonic vortices formed early in the jet development and seemed to stagnate before sliding into one another with little net rotation. This can be observed in our model when there is initially a low amplitude but high lateral irregularity, so that coalescence takes place before the vortices develop fully.

In their experiments on high Reynolds number turbulent flows, Brown & Roshko estimated the visual spreading rate of the mixing layer in homogeneous flow. This was equivalent to

$$d(H/\lambda)/dT = 0{\cdot}38.$$

This line is shown in figure 13 (case 1) and is seen to be approximately the growth rate during the modelled pairing process. This could indicate that a continual

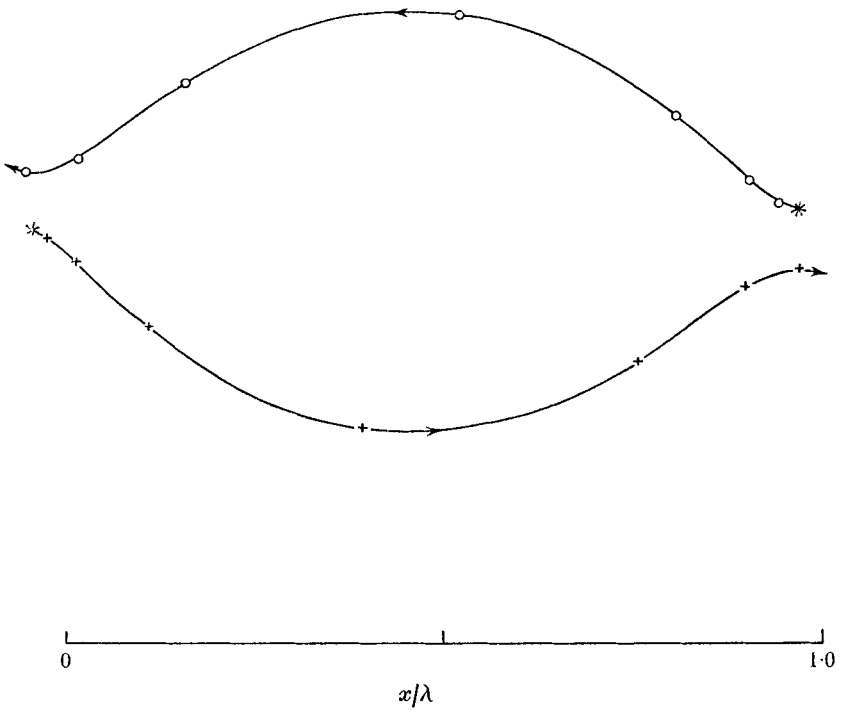

FIGURE 18. Typical paths of the members of two equi-spaced infinite rows of vortices. O, +, equal time intervals; *, initial positions.

repeated coalescence of eddies could account for the spreading rate of the turbulent mixing layer.

The model presented here is basically inviscid and requires no turbulent diffusion mechanism. This is in agreement with the ideas presented by Brown & Roshko, and also by Winant & Browand, where it is the amalgamation process which entrains the fluid by trapping irrotational fluid between the coalescing structures. The smaller instabilities embedded in the larger structures do not add to the basic ingestion of fluid. Recently, Moore & Saffman (1975) have suggested an alternative process for the growth of the large eddy structure in the mixing layer. They consider that the large eddy is growing continuously by turbulent entrainment and the structures reach such a size that any weak vortex gets torn apart by the action of its neighbours, thus satisfying the requirement for the number of eddies to decrease.

Moore & Saffman have two objections to the process of vortex amalgamation described by Winant & Browand. One is that Brown & Roshko did not observe the process. But, although it is not discernible from their shadowgraphs, they suggest in their recent (1974) paper that amalgamation events can be seen by plotting eddy trajectories on an x,t diagram. The second objection is that the inviscid assumption gives a vorticity relation which is inconsistent with the similarity laws. However, this was based on calculations assuming vortices of constant cross-sectional shape. But such a regular geometry is not observed here nor was it seen by Winant & Browand.

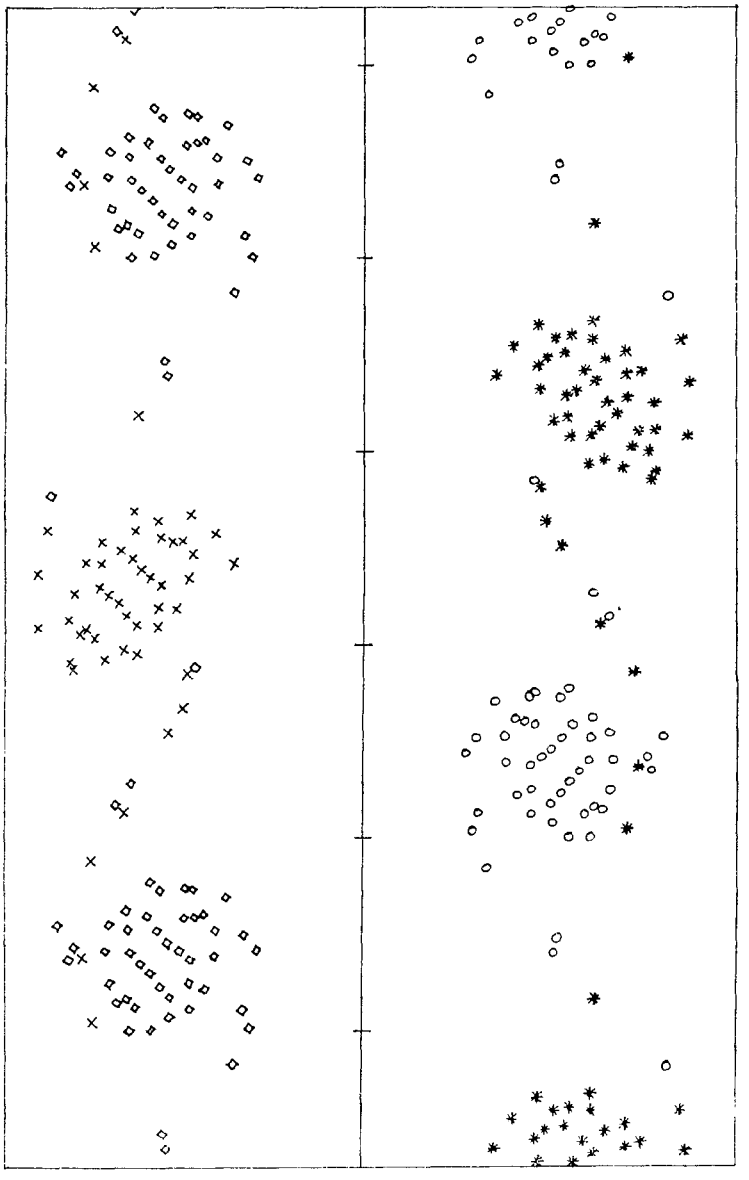

FIGURE 19. The sinuous form of a developing asymmetric jet. $T = 0{\cdot}666$.

The similarity law requires that the vorticity should decrease linearly with downstream distance. From the form of the vortical structures during the amalgamation shown in figure 10, it is possible tentatively to estimate the changes in mean vorticity. This is shown in figure 20 for four points during the pairing. The vorticity does show a linear relationship with T (equivalent to x) and so this inviscid process does not seem to be inconsistent with the similarity law. This decrease in vorticity would occur because of the entrainment of irrotational fluid as discussed above.

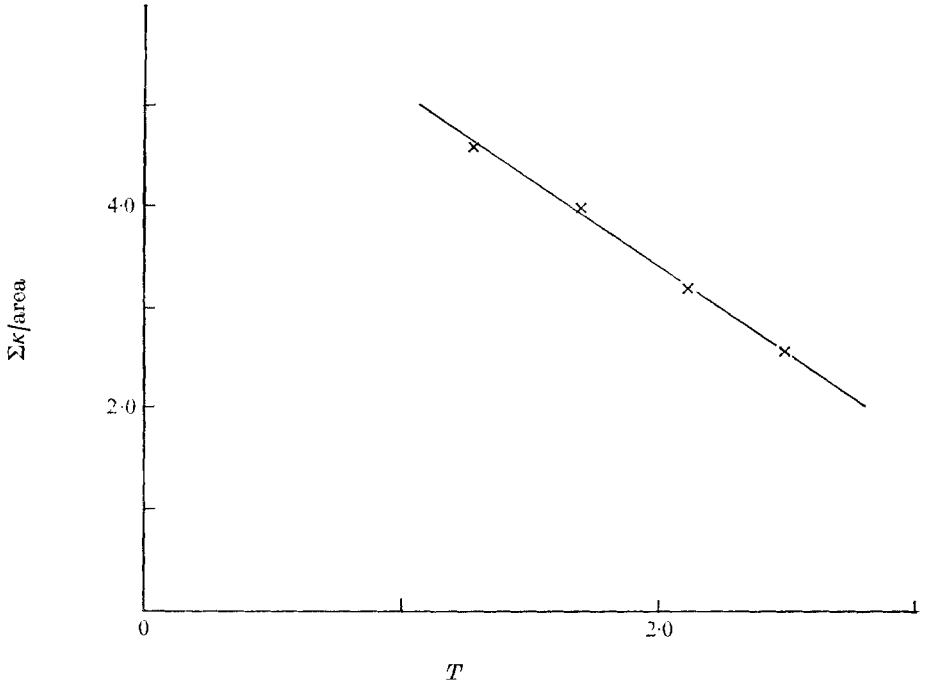

FIGURE 20. The estimated variation of mean vorticity with time.

However, the destruction of a weak eddy by the gradual removal of its vorticity by its neighbours can be demonstrated using the model presented here. The essential requirement is that the stronger eddy should also be larger. This can be achieved by specifying a length of shear layer which includes both a short wavelength and a long wavelength. These roll up at differing rates to form unequal structures. It is found that the larger vortex continuously rotates about its own axis and, whilst elongated in the flow direction, as described previously, is able gradually to ingest the vorticity of the weaker. The 'centre' of vorticity of the large structure remains unchanged. However, this does take a long time ($T = 3{\cdot}2$ based on the longer wavelength) and also requires a very regular array ($\delta = 0$); otherwise coalescence by rotation and pairing occurs first.

5. Conclusions

A model of the development of large eddies in a shear layer is shown to require some representation of the distribution of the vorticity. The motion of two discrete line-vortex pairs is either cyclic or non-cyclic depending solely on the initial conditions. The motion of typical members of two equi-spaced infinite rows of vortices is never cyclic. There is no tendency for such vortices to coalesce. The shear layer itself must be modelled if eddy evolution is to be visualized effectively.

The observed development of our model shear layer is consistent with many features previously described. Apart from the situation where there is a very

large initial layer thickness, it is seen that after coalescence the structures formed are approximately independent of the initial conditions. The amalgamation process is seen to be relatively abrupt and so would be likely to be a most effective noise source; but controlling the process by means of the initial conditions does not seem feasible.

It is seen that the pairing process is a likely mechanism for the growth of a turbulent mixing layer. The irregularities caused in the layer by any coalescence would be sufficient to provoke further pairings, thus ensuring continual amalgamation events to produce the smooth linearly growing mixing layer. The growth mechanism proposed by Moore & Saffman could also occur if the conditions were such that the irregularities in strength were more prominent than those in lateral spacing. It seems possible that both mechanisms could be occurring at different points in the layer, but we think vortex pairing to be a more probable mechanism of growth.

This work is part of the research programme sponsored at Cambridge University by Rolls-Royce (1971) Ltd. The help and encouragement of Professor J. E. Ffowcs Williams is gratefully acknowledged. The author also wishes to thank the Director of Computing Service for use of the facilities of the University Computer.

REFERENCES

BATCHELOR, G. K. 1970 *An Introduction to Fluid Dynamics*, chap. 7. Cambridge University Press.

BROWN, G. L. & ROSHKO, A. 1974 On the density effects and large structure in turbulent mixing layers. *J. Fluid Mech.* **64**, 775–816.

CHORIN, A. J. & BERNARD, P. S. 1972 Discretization of a vortex sheet, with an example of roll-up. *Univ. Calif. Rep.* FM-72-5.

CROW, S. C. & CHAMPAGNE, F. H. 1971 Orderly structure in jet turbulence. *J. Fluid Mech.* **48**, 547–591.

FREYMUTH, P. 1966 On transition in a separated laminar boundary layer. *J. Fluid Mech.* **25**, 683–704.

HAMA, F. R. & BURKE, E. R. 1960 On the rolling-up of a vortex sheet. *Univ. Maryland Tech. Note*, BN-220.

KINNS, R. 1975 Binaural source locations. *J. Sound Vib.* (to appear).

LAMB, H. 1924 *Hydrodynamics*. Cambridge University Press.

LAU, J. C. & FISHER, M. J. 1975 The vortex-street structure of turbulent jets. Part 1. *J. Fluid Mech.* **67**, 229–338.

LAUFER, J. 1974 On the mechanism of noise generation by turbulence. *Univ. Southern Calif. School Engng Rep.* USCAE 125.

LIGHTHILL, M. J. 1952 On sound generated aerodynamically. *Proc. Roy. Soc.* A **211**, 564–587.

LOVE, A. E. H. 1894 On the motion of paired vortices with a common axis. *Proc. Lond. Math. Soc.* **25**, 185–194.

MICHALKE, A. 1963 On the instability and non-linear development of a disturbed shear layer. *Hermann-Föttinger-Inst. Strömungstech. Tech. Univ. Berlin Rep.* AF 61(052)-412 TN-2.

MICHALKE, A. 1970 The instability of free shear layers: a survey on the state of the art. *DLR Mitt.* no. 70–74.

MOORE, D. W. 1971 The discrete vortex approximation of a finite vortex street. *Calif. Inst. Tech. Rep.* AFOSR-1804-69.

MOORE, D. W. & SAFFMAN, P. G. 1975 The density of organized vortices in a turbulent mixing layer. *J. Fluid Mech.* **69**, 465–473.

ROCKWELL, D. O. & NICCOLLS, W. O. 1972 Natural breakdown of planar jets. *Trans. A.S.M.E.* D **94**, 720–730.

ROSENHEAD, L. 1932 The formation of vortices from a surface of discontinuity. *Proc. Roy. Soc.* A **134**, 170–192.

WINANT, C. D. & BROWAND, F. K. 1974 Vortex pairing: a mechanism of turbulent mixing-layer growth at moderate Reynolds number. *J. Fluid Mech.* **63**, 237–255.